INDIAN JOURNAL OF SCIENCE AND TECHNOLOGY

RESEARCH ARTICLE

High-Performance and Robust Field-Oriented Control of IPMSM Drive Over Wide Speed Operation by PI and Fuzzy Intelligent Controllers

Jaydeepsinh C Baria[1]*, Kuldip Patel[2], Darshankumar C Dalwadi[3], C Dalwadi[3]

1 Ph.D Research scholar, Gujarat Technological University, India
2 BVM Engineering College, V. V. Nagar, Anand, India
3 Associate Professor, BVM Engineering College, Anand, India

OPEN ACCESS

Received: 06-04-2023
Accepted: 15-06-2023
Published: 04-07-2023

Citation: Baria JC, Patel K, Dalwadi DC, Dalwadi C (2023) High-Performance and Robust Field-Oriented Control of IPMSM Drive Over Wide Speed Operation by PI and Fuzzy Intelligent Controllers. Indian Journal of Science and Technology 16(26): 1947-1957. https://doi.org/10.17485/IJST/v16i26.776

* **Corresponding author**.

jcbaria1982@gmail.com

Funding: None

Competing Interests: None

Published By Indian Society for Education and Environment (iSee)

ISSN
Print: 0974-6846
Electronic: 0974-5645

Abstract

Objectives: This paper simulates a high-performance PI and FLC-based controller for an IPMSM drive in which the speed should closely follow the reference speed and voltage-current trajectory with different conditions like load disturbance, variation in circuit parameters, and control strategy. In FOC, the PI and fuzzy controller are used for sliding mode control. This controller generates the d-axis current (Id) and q-axis current (Iq), which control the torque and magnetic field vector for each stator winding, so the speed of the motor can be effectively controlled. **Methods:** In this paper, we used two loops: one is the outer speed loop, and another is the inner loop called the current loop, which generates the pulses for the inverter. The optimal behavior of the controllers is designed based on the Maximum Torque per Ampere (MTPA) method for stand-still to base speed operation and the Field Weakening (FW) method for the above base speed operation. The mathematical model of the IPMSM motor can be derived from its dynamic d-q model. This proposed drive system is simulated in MATLAB-Simulink software with different conditions like speeds and loads. Moreover, the fixed-gain PI controller is mostly affected by the step change in reference speed, circuit parameters, and load condition. The accurate speed control of the drive becomes a complex issue due to the non-linear coupling between the stator current and rotor and the non-linearity in the torque. Therefore, the fuzzy controller is more popular in high-performance IPMSM drives. **Novelty:** In this paper, the FLC is used as a speed controller, and the proposed control scheme reduces the computation for real-time implementation. The hysteresis current controllers are used, and outputs are given to logic, which is used to switch ON and OFF the inverter. The robustness of the FLC-based drive is verified by theoretical and simulation results. In this paper, the three inputs to the FLC are: is the change in rotor speed, ω_r is rotor speed, and Δe is the change in speed error. Fuzzy rules are developed by different membership functions used to obtain the optimized value (I_d^* and Iq*), which gives precise speed control under different operating

conditions over a wide speed range.

Keywords: Interior Permanent Magnet Synchronous Motor (IPMSM); Fuzzy Logic Controller (FLC); proportionalintegral (PI) Maximum Torque per Ampere (MTPA); Field Weakening (FW); Vector Control; fieldoriented control (FOC); Hysteresis Current Controller

1 Introduction

IPMSM was introduced in 2001, and it is now widely accepted as an efficient alternative to AC induction motors. A lot of research has been done on PM material, power electronics devices, and control topologies, so we can develop an efficient IPMSM motor that offers accurate speed control over a wide range of speeds, high efficiency, is compact, has low copper losses, has a long bearing grease life, and has a high-power density. So IPMSM is most suitable for loads like electric vehicles, elevators, and traction, in which space limitations are important [1–4].

IPMSM offers good control over a wide speed range. This is done by the Maximum Torque Per Ampere (MTPA) and Field Weakening (FW) algorithms. We control the speed from zero to the base (rated) speed by MTPA and beyond the base speed by the FW methodology. [2,3] IPMSM has permanent magnets buried inside the rotor structure. Its rotor surface will become smooth, and the air gap will be reduced. Therefore, it is suitable for high-speed operation. The d-axis inductance and q-axis inductance are not equal for IPMSM. It will give us an extra torque produced by the d-axis current called "reluctance torque." [5] Therefore, in MTPA, we get maximum torque per unit current; this is how we can reduce the copper loss in IPMSM to its minimum and get better efficiency [3,4]. We will reduce the flux by negative d-axis current to go beyond the base speed of operation. The motor parameters play a crucial role in the FW region because the voltage constraint depends on the motor parameter [6].

The rotor core around the permanent magnets is saturated. The armature reaction affects the air gap flux in IPMSM. Due to this, the reluctance parameters of IPMSM are varied. Hence, the dynamic and steady-state performance of IPMSM are affected. Its control in high-performance industrial applications requires special attention. The precise speed control of an IPMSM drive becomes very difficult and complex due to the non-linear coupling between stator current and rotor speed. Drive gives non-linearity in the electromagnetically developed torque.

As we know, proportional-integral (PI) controllers were used for speed and current control purposes. The biggest disadvantage of the PI controller is its dependence on dynamic and machine parameter variations. So, PI controller performance has significantly deteriorated during the dynamic performance of the drive (like overshoot, undershoot, more settling time, etc.). So, it is one of the main concerns for high-performance and robust drive applications. Thus, the PI controller is replaced by the FLC due to its many advantages. FLC is utilized by fuzzy rules to ensure optimum drive performance under different operating and disturbance conditions [5,7–10].

High-performance drives are used in machine tools, mills, rolling, air conditioning, washing machines, EVs, robotics, etc., which require an accurate and fast dynamic response. The dynamic response of an IPMSM drive can be improved using field-oriented control, also known as vector control, where three-phase motor variables are transformed to stationary DQ references by the Park and Clark transformation. So, speed and torque can be controlled individually by I_d and I_q. Due to this, the IPMSM drive will give a good dynamic response and work like a separately excited DC motor. To verify the robustness of the proposed controller, the performance of the IPMSM drive is investigated by simulation at different operating conditions. The performance of the IPMSM drive using different controllers is also measured in terms of the THD of the stator winding current and speed response.

Nomenclature
R_S - Per phase Stator Resistance
i_d - d-axis stator current
i_q - q-axis stator current
L_d - d-axis stator inductance
L_q - q-axis stator inductance
ω_e - rotor speed
Φ_d - flux linkage along d-axis
Φ_q - flux linkage along q-axis
Φ_{PM} - flux linkage due to Permanent Magnet
P - Number of Pole Pairs
θ_r - phase shift

1.1 Mathematical Model of IPMSM

The mathematical model for the vector control of the IPMSM can be derived from its dynamic d-q model, which can be obtained from a well-known induction machine model with the equations of damper winding and field current dynamics removed. The synchronously rotating rotor reference frame is chosen so that the stator winding quantities are transformed into the synchronously rotating reference frame that is revolving at rotor speed. The consequence is that there is zero speed differential between the rotor and stator magnetic fields. The stator q-axis and d-axis windings have a fixed phase relationship with the rotor magnet axis, which is the d-axis in the modelling. A mathematical model of the IPMSM is used to simulate the behaviour of the machine in Matlab or Simulink. The model is expressed in the d-q rotor reference frame, where the d-axis is aligned with the rotor flux linkage as shown in Figure 1 [11,12].

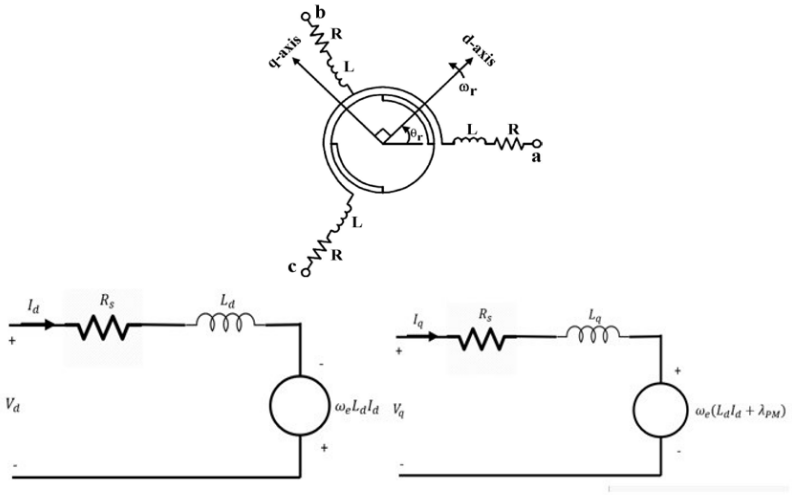

Fig 1. The Vector Diagram for DQ transformation and equivalent circuit in the DQ-axis

The stator voltages for 3 phases can be written as below:

$$v_a = R_s i_a + L_s \frac{d}{dt} i_a - \omega_e \Phi_{PM} sin(\theta_r) \tag{1}$$

$$v_b = R_s i_b + L_s \frac{d}{dt} i_b - \omega_e \Phi_{PM} sin\left(\theta_r - \frac{2\pi}{3}\right) \tag{2}$$

$$v_c = R_s i_c + L_s \frac{d}{dt} i_c - \omega_e \Phi_{PM} sin\left(\theta_r + \frac{2\pi}{3}\right) \tag{3}$$

Equations (4) and (5) are Dynamic equations of IPMSM in a synchronously rotating d-q referencing frame obtained by clerk-perk transformation. Some assumptions will be taken for convenience.

- The induced EMF is Sinusoidal.
- Saturation and Core losses in the rotor are negligible.
- There is no damper winding on the rotor.

$$v_d = R_S i_d + L_d \frac{di_d}{dt} - \omega_e \Phi_q \tag{4}$$

$$v_q = R_S i_q + L_q \frac{di_q}{dt} + \omega_e \Phi_d \tag{5}$$

$$\Phi_d = L_d i_d + \Phi_{PM} \tag{6}$$

$$\Phi_q = L_q i_q \tag{7}$$

The Equivalent circuit of the PMSM in DQ- axis derived using DQ modeling method is shown in Figure 1.

$$T_e = \frac{3P}{2}(\Phi_{PM} i_q + (L_d - L_q) i_d i_q) \tag{8}$$

The first term in Equation (8) represents the torque due to the permanent magnet buried in the rotor, and the second term represents the reluctance torque developed due to the interaction of d- axis and q-axis current.

1.2 Maximum torque per Ampere (MTPA) Control

Maximum torque per Ampere control generates the reference d-axis current (i_d) and q-axis current (i_q), to produce maximum torque per unit current. The condition for MTPA trajectory can be derived from Equation (8) as follows. [12]

$$\frac{\partial T_e}{\partial i_q} = 0$$

$$\Phi_{PM} + (L_d - L_q)\, i_q \frac{\partial T_e}{\partial i_q} + (L_d - L_q)\, i_d = 0 \tag{9}$$

The relation between stator phase current and current in the d-q reference frame is

$$i_s = \sqrt{i_d^2 + i_q^2} \tag{10}$$

Using equation (8)

$$\frac{\partial i_d}{\partial i_q} = -\frac{i_q}{i_d} \tag{11}$$

Solving equations (7) and (9)

$$i_d = \frac{\Phi_{PM}}{2\,(L_d - L_q)} + \sqrt{\frac{{\Phi_{PM}}^2}{4(L_d - L_q)^2} + i_q^2} \tag{12}$$

The trajectory of the MTPA curve, the voltage limit ellipse, the current limit curve, and the constant torque curves are shown in Figure 3.

The voltage constraints for the drive system are satisfied for below-base speed operation. The operating point of the drive system is located along the MTPA trajectory shown in Figure 2. The intersecting point of the constant torque curve and MTPA trajectory is the operating point, which is at a minimum distance from the origin. This distance represents the stator current. In other words, MTPA trajectory leads to the required torque by the minimum current. Therefore, the copper loss is reduced and the efficiency of the drive system can be maximized [12,13].

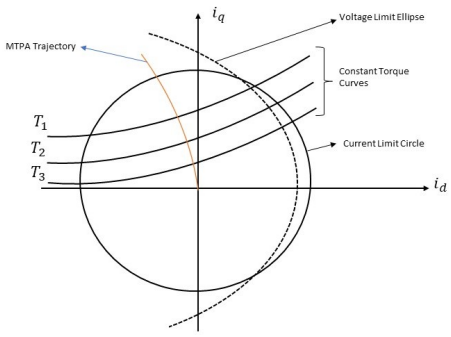

Fig 2. Limit Curves in MTPA Operating Region

1.3 Field Weakening (FW) Control

When we operate our motor beyond the rated speed, we need to care about the Voltage and Current constraints [13]. The Current constraint and Voltage constraint are expressed using Equation (10) and (11) respectively.

$$I_s = \sqrt{I_d^2 + I_q^2} \leq I_{sm} \tag{13}$$

$$V_s = \sqrt{\upsilon_d^2 + \upsilon_q^2} \leq V_{sm} \tag{14}$$

Where I_{sm} and V_{sm} are available maximum current and voltage respectively.

Put the values of v_d and v_d in equation (14), and we get

$$V_s = \sqrt{\left(R_S i_d + L_d \frac{di_d}{dt} - \omega_e \Phi_q\right)^2 + \left(R_S i_d + L_d \frac{di_d}{dt} + \omega_e \Phi_d\right)^2} \leq V_{sm} \tag{15}$$

To make the analysis simple, we consider only steady-state terms in the voltage constraint equation and ignore the resistive drop.

$$V_s = \sqrt{(\omega_e \Phi_d)^2 + (\omega_e \Phi_d)^2} \leq V_{sm} \tag{16}$$

From Equations (7) and (8), we get

$$V_s = \sqrt{(\omega_e L_q i_q)^2 + (\omega_e (L_d i_d + \Phi_{PM}))^2} \leq V_{sm} \tag{17}$$

After simplification,

$$(L_q i_q)^2 + (L_d i_d + \Phi_{PM})^2 \leq \left(\frac{V_{sm}}{\omega_e}\right)^2 \tag{18}$$

Equation (13) represents the current limit circle with radius I_s and center at the origin.

Equation (18) represents the voltage ellipse centered at $(0, -\frac{\Phi_{PM}}{L_d})$ and contracts as the speed of the rotor increases.

When the operation is beyond base speed, the field weakening is employed so that the stator voltage will remain within the limit given by the equation (15). The d-axis and q-axis current is controlled such that they can satisfy the machine voltage limit given by

$$\upsilon_o = \sqrt{\upsilon_{do}^2 + \upsilon_{qo}^2} \leq V_{om} \tag{19}$$

Where, $\upsilon_{do} = -\omega_e L_q i_q$, $\upsilon_{qo} = \omega_e(L_d i_d + \Phi_{PM})$ and $V_{om} = V_{sm} - R_S I_{sm}$.

The relationship between i_d and i_q can be derived by equation (17) by replacing V_{sm} with V_{om} to induce the effect of the Stator Resistance drop. Therefore,

$$i_d = -\frac{\Phi_{PM}}{L_d} + \frac{1}{L_d}\sqrt{\frac{\upsilon_{om}^2}{\omega^2} - (L_q i_q)^2} \tag{20}$$

To control the current vector according to equation (20), the terminal voltage should be kept within V_{sm} in a steady state. The intersection between the current limit and voltage limit trajectories at each speed provides the respective current limit for producing maximum torque at each operating speed. The operating point is located along the voltage limit curve. Therefore, the voltage limit curve decides the minimum current required to produce the desired torque. The copper loss is also reduced in the FW region[2,3]. These limit values are given by equations (21) and (22) respectively.

$$i_{dv} = -\frac{\Phi_{PM} L_d}{L_d^2 - L_q^2} + \frac{1}{L_d^2 - L_q^2}\sqrt{\Phi_{PM}^2 L_d^2 - (L_d^2 - L_q^2)(I_{sm}^2 L_q^2 + \Phi_{PM}^2 - \frac{V_{sm}^2}{\omega^2})} \tag{21}$$

$$i_{qv} = \sqrt{I_{sm}^2 - i_{dv}^2} \tag{22}$$

The trajectory of the MTPA curve, the current limit curve, constant torque curves at different load, and the Voltage limit curve in the FW region is shown in Figure 2.

2 Methodology

2.1 Design of PI Controller

Figure 3 shows the proposed PI controller block diagram, which is implemented in MATLAB-Simulink using the MATLAB Toolbox. The speed command is given to the drive system. Commanded speed is compared with sensing speed and generates the error signal, which is given to the PI controller and generates the torque command. Three-phase current is converted to two stationary d-q components by the Clark and Park transformation. The actual value of the q-axis and d-axis current is compared with a reference value of the q-axis and d-axis current (Id* and Iq*), and an error will be sent to the current controller (PI controller). So, we can get the reference values of Vq* and Vd*, which will help us do inverse Clark and Park transformations, and finally, we can get three-phase components. For the above two conversions, we need a rotor angle. The SVPWM (space vector pulse width modulation) technique is used as a pulse width modulation technique. SVPWM drives the inverter gate signals, which give controlled voltage and frequency to the IPMSM. Both the speed and current controllers are tuned by the transfer function-based PI tune approach[14]

2.2 Fuzzy logic controller

Figure 3 shows the proposed FLC implemented in MATLAB-Simulink using the Fuzzy Logic Toolbox. The inputs to the FLC are speed error, change in speed error, and actual speed. The outputs of FLC are d-axis current (Id) and q-axis current (Iq). The membership functions for inputs and outputs are defined, and fuzzy rules are made to get the reference values of the q-axis and d-axis current (Id* and Iq*). The inputs and outputs of FLC are scaled by appropriate gains so that the system performs efficiently. The hysteresis current controller is used as the gate signal of the inverter. In this control scheme, the Id and Iq currents are controlled, which control the motor speed and torque[15–18].

The fuzzy rules are as under,

Rule 1: **If** $\Delta\omega$ is PH (positive high), **then** i_q is PH (positive high), **and** i_d is PH (positive high).

Rule 2: **If** $\Delta\omega$ is PL (positive low), **then** i_q is PL (positive low), **and** i_d is PL (positive low).

Rule 3: **If** $\Delta\omega$ is NH (negative high), **then** i_q is NH (negative high), **and** i_d is NH (negative high).

Rule 4: **If** $\Delta\omega$ is NL (negative low), **then** i_q is NL (negative low), **and** i_d is NL (negative low).

Rule 5: **If** $\Delta\omega$ is ZE (zero) **and** ω_r is WR (within range), **then** i_q is NC (not changed), **and** i_d is NC (not changed).

Rule 6: **If** ω_r is PAR (positive above rated) **or** NAR (negative above rated), **then** i_q is NL (negative low), **and** i_d is AR (above rated).

Rule 7: **If** $\Delta\omega$ is ZE (zero) **and** Δe is PI (positive increase), **then** i_q is PL (positive low), **and** i_d is PL (positive low).

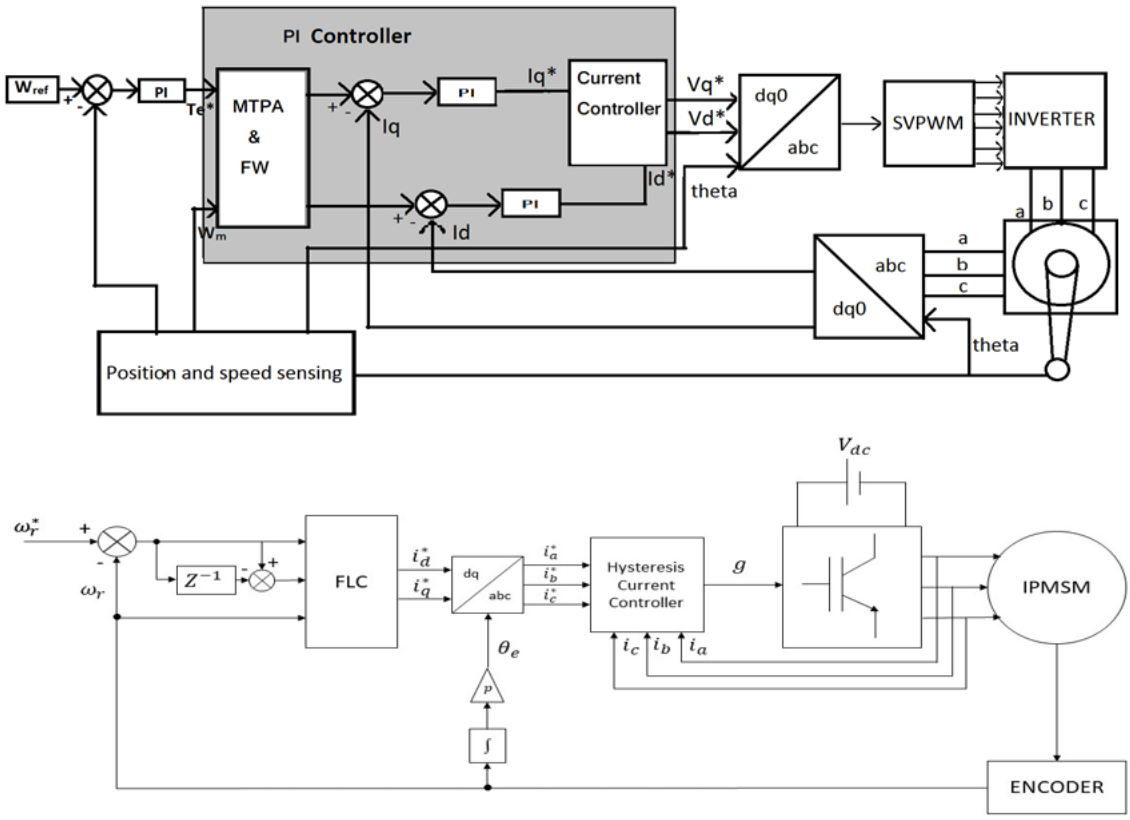

Fig 3. Proposed Block diagram for PI and FLC controller

Rule 8: **If** $\Delta\omega$ is ZE (zero) **and** Δe is NI (negative increase), **then** i_q is NL (negative low), **and** i_d is NL (negative low).
Where,
$\Delta\omega$ is the change in rotor speed,
ω_r is rotor speed,
Δe is the change in speed error
IPMSM motor parameters are given in Table 1

3 Results and Discussion

The performance of the proposed controllers has been investigated in MATLAB simulation at various dynamic operating conditions. The simulation results are below. The simulation for both PI and fuzzy is initiated by setting the constant 10 Nm load torque.

In the PI controller, the speed is undershot at starting 1000 rpm, but after giving step input to 1500 rpm and 2000 rpm, the speed is overshot up to 1526 rpm and 2027 rpm, as shown in Figure 4. where the FLC's minimum overshoot in speed is observed at different step inputs. At 1000, 1500, and 2000 rpm step inputs, the actual speed is 1008, 1508, and 2011 rpm, as seen in Figure 4. FLC controllers closely follow the reference speed. The effectiveness of the FLC is proven by the minimum overshoot concerning reference speed. With both controllers, the desired speed is achieved.

The electromagnetic torque responses by PI and FLC are shown in Figure 5. As we discussed in the mathematical model, the electromagnetic torque is positive when the Q-axis current component is positive and the D-axis current component is negative. Iq will control torque, so in both controllers, Iq and torque response behaviour are almost the same. where Id will control the stator flux, while speed above the rated speed value of Id is more negative, as shown in Figure 6.

As a result, the motor's starting torque peak was almost 88 N-m when we raised the reference speed from 0 to 1000 rpm, and it reduced from 9.6 N-m to 9.1 N-m in 0.15 seconds. When the speed was raised to 1500 rpm, the torque peak was 55.5 N-m,

Table 1. IPMSM Simulation Parameters

Parameter	Parameter Value
Number of Pole Pairs	4
Stator Resistance	0.138 Ω
Permanent Magnet Flux Linkage	0.171 Vs
	0.00251 H
q-axis Inductance	0.00617H
Line Voltage (rms)	440 V
Phase Current (rms)	60 A
Base Speed	1500 rpm
Rated Torque	50 Nm
Friction Coefficient	0.00001
Rotor Inertia	0.04357 kg.m^2

but it took 0.10 seconds to reach 9.3 N-m to 9.6 N-m. When the speed was raised to 2000 rpm again, the torque peak was at 55.3 N-m and reached 9.3 N-m to 9.5 N-m in 0.15 seconds, as shown in Figure 5. Increasing reference speed caused the torque of the motor to reach its maximum before settling down to almost 10 N-m; this was noted in the waveforms and shown in the observation Table 2. In PI controller actual speed taken some time to reach the reference speed, during this time torque ripple is observed in Figure 5.

The torque ripple is a little higher in FLC as compared to PI controllers. In, the PI controller the actual speed is reached to reference speed but in the case of FLC actual speed never reaches to reference speed due to defining fuzzy rules in the controller which continuously give errors between them.

The harmonic spectrum for three-phase stator current at different step speeds by PI and FLC are shown in Figure 8 which are at an acceptable level of THD.

Table 2 contains the important observations from the simulation, both the controllers are simulated at various dynamic, transients (rise time, delay time, settling time) and steady-state responses (Torque ripple, current ripple (THD), Steady State Error (e_{ss}) in Speed) conditions.

In accordance with Table 2, a motor's performance in dynamic circumstances (differences in speed, torque, frequency, etc.) showed that FLC worked well under transient conditions, but when the conditions were in a steady state, PI worked well. That is observed in Figures 4 and 5.

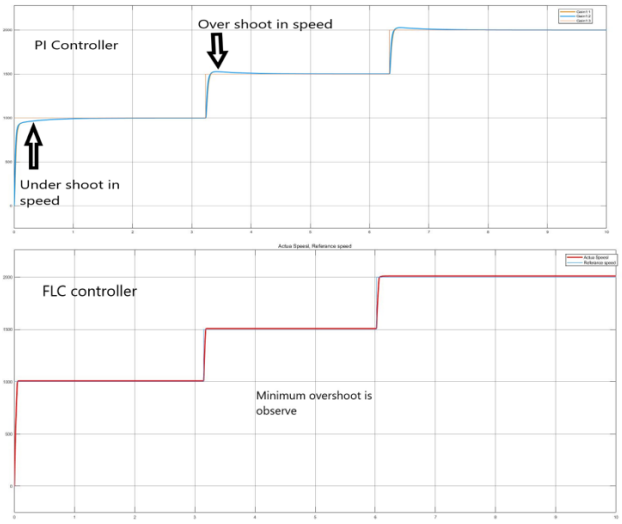

Fig 4. Speed Response by PI and FLC controllers

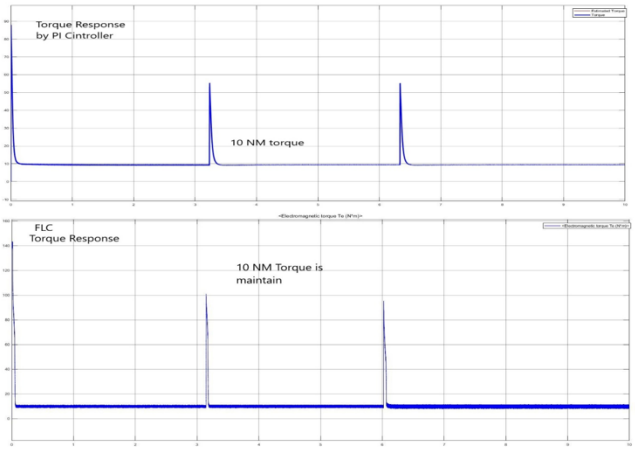

Fig 5. Torque response by PI and FLC controllers at different speeds

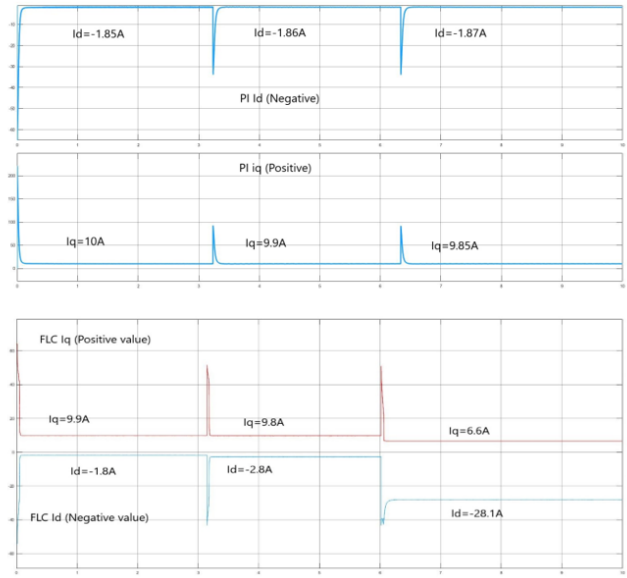

Fig 6. I_d and I_q current response by PI and FLC at different speeds

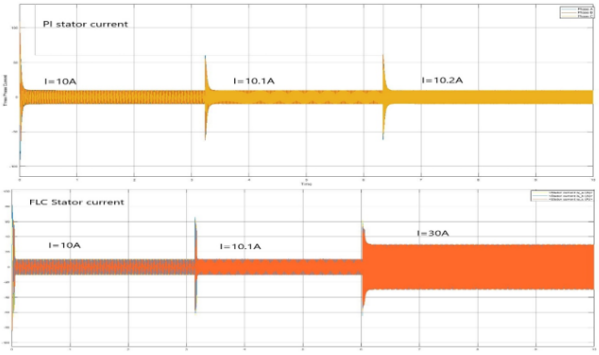

Fig 7. Three-phase stator current Response by PI and FLC controller at different speeds

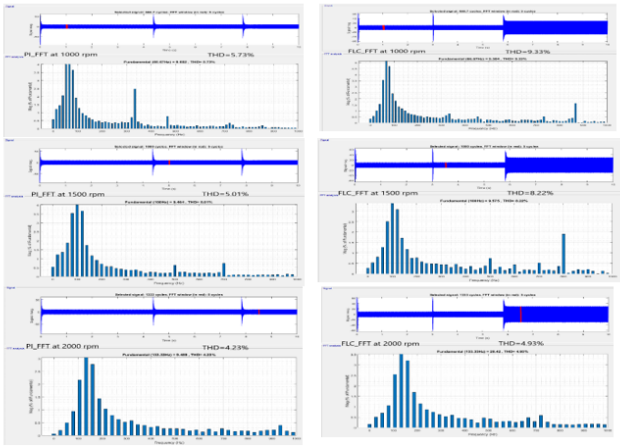

Fig 8. THD at a different speed

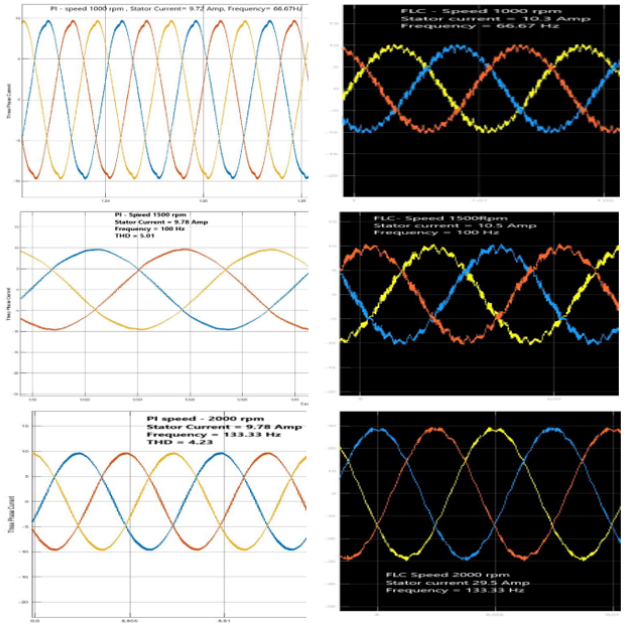

Fig 9. Three-phase stator current Response by PI and FLC controller at different speeds with two to three cycles

Table 2. Simulation Observation and Analysis

Speed Change	**0 to 1000 rpm**		**1000 to 1500 rpm**		**1500 to 2000 rpm**	
Controller	**PI**	**Fuzzy**	**PI**	**Fuzzy**	**PI**	**Fuzzy**
Transient Response Parameters						
Rise Time	0.06 sec	0.043 sec	0.04 sec	0.03 sec	0.03 sec	0.03 sec
Delay Time	0.026 sec	0.019 sec	0.03 sec	0.019 sec	0.032 sec	0.01 sec
Settling Time	2 sec	0.04 sec	1.72 sec	0.041 sec	1.82 sec	0.04 sec
Steady State Response Parameters						
Torque Ripple	6.45%	24%	3.19%	25.64%	2.12%	38.34%
THD (Current)	5.73%	9.33%	5.01%	8.22%	4.23%	4.93%
Steady State Error (e_{ss}) in Speed	0.1%	0.8%	0.1%	0.53%	0.1%	0.55%

4 Conclusion

The PI and FLC controllers for IPMSM drives are simulated in this paper. The FLC has been optimized by fuzzy rules that reflect the minimum settling time, minimum overshoot/undershoot, and minimum steady-state error at different step speeds as compared to the PI controller. The PI controller has less torque ripple as compared to the FLC. Stator current THD is within a limit in both controllers. The FOC scheme has been incorporated into the integrated drive system to achieve high performance. So, we can conclude that the PI controller is superior under steady-state conditions and the fuzzy logic controller is better under transient conditions.

Acknowledgement

We would thank Electrical engineering department of Birla Vishvakarma Mahavidyalaya for providing MATLAB licensed version software for simulation work. We would also thank Dr. Rukmi Dutta, Associate Professor, University of south wales, Sydney, Australia for providing motor data during training.

References

1) Eldeeb HM, Abdel-Khalik AS, Hackl CM. Dynamic Modeling of Dual Three-Phase IPMSM Drives With Different Neutral Configurations. *IEEE Transactions on Industrial Electronics*. 2019;66(1):141–151. Available from: https://doi.org/10.1109/TIE.2018.2823684.
2) Moradian M, Soltani J, Najjar-Khodabakhsh A, Markadeh GRA. Adaptive Torque and Flux Control of Sensorless IPMSM Drive in the Stator Flux Field Oriented Reference Frame. *IEEE Transactions on Industrial Informatics*. 2019;15(1):205–212. Available from: https://doi.org/10.1109/TII.2018.2808521.
3) Nan Z, Dejun Y. Research on MTPA control of IPMSM Drive Using Online Parameter Identification Method. *2020 5th Asia Conference on Power and Electrical Engineering (ACPEE)*. 2020;p. 689–693. Available from: https://doi.org/10.1109/ACPEE48638.2020.9136376.
4) Mitsubishi Electrical inverter, "IPM TECHNICAL NOTE". .
5) Mishra A, Dubey G, Joshi D, Agarwal PP, Sriavstava SP. A Complete Fuzzy Logic Based Real-Time Simulation of Vector Controlled PMSM Drive. *2018 2nd IEEE International Conference on Power Electronics, Intelligent Control and Energy Systems (ICPEICES)*. 2018;p. 809–814. Available from: https://doi.org/10.1109/ICPEICES.2018.8897373.
6) Liu Z, Zhang L, Huang D, Liu E, Zhu Z, Wang X. A New Flux Weakening Control Strategy for IPMSM (Interior Permanent Magnet Synchronous Machine) in Automotive Applications. *SAE Technical Paper Series*. Available from: https://doi.org/10.4271/2020-01-0466.
7) Sain C, Banerjee A, Biswas PK, Balas VE. Performance optimisation for closed loop control strategies towards simplified model of a PMSM drive by comparing with different classical and fuzzy intelligent controllers. *International Journal of Automation and Control*. 2020;14(4):469. Available from: https://www.inderscienceonline.com/doi/epdf/10.1504/IJAAC.2020.108281.
8) Sakunthala S, Kiranmayi R, Mandadi PN. Investigation of PI and Fuzzy Controllers for Speed Control of PMSM Motor Drive. *2018 International Conference on Recent Trends in Electrical, Control and Communication (RTECC)*. 2018;p. 133–136. Available from: https://doi.org/10.1109/RTECC.2018.8625636.
9) Hu T, Zhang X. Simulation of PMSM Vector Control System Based on Fuzzy PI Controller. *2019 IEEE International Conference on Power, Intelligent Computing and Systems (ICPICS)*. 2019;p. 111–114. Available from: https://doi.org/10.1109/ICPICS47731.2019.8942439.
10) Hoai HK, Chen SC, Chang CF. Realization of the Neural Fuzzy Controller for the Sensorless PMSM Drive Control System. *Electronics*. 2020;9(9):1371. Available from: https://doi.org/10.3390/electronics9091371.
11) Kongchoo N, Santiprapan P, Jindapetch N. Mathematical Model of Permanent Magnet Synchronous Motor. *Asia Pacific Conference on Robot IoT System Development and Platform*. 2020. Available from: https://ipsj.ixsq.nii.ac.jp/ej/?action=repository_uri&item_id=210331&file_id=1&file_no=1.
12) Zhuoyong W, Xiaodong Y, Jiakang L, Liangxu X, Hui T, Ke L. Research on IPMSM Control Based on MTPA. *Procedia Computer Science*. 2022;208:635–641. Available from: https://doi.org/10.1016/j.procs.2022.10.087.
13) Lan Z, Shen F, Zhu G, Chen C, Li L, Cao C. A Novel Control Method of Improved Flux-Weakening Trajectory for IPMSM. *2019 22nd International Conference on Electrical Machines and Systems (ICEMS)*. 2019;p. 1–6. Available from: https://doi.org/10.1109/ICEMS.2019.8921440.
14) Ekanayake S, Dutta R, Rahman MF, Xiao D. Direct torque and flux control of interior permanent magnet synchronous machine in deep flux-weakening region. *IET Electric Power Applications*. 2018;12(1):98–105. Available from: https://doi.org/10.1049/iet-epa.2017.0147.
15) Baria JC, Patel K, Dalwadi DC. Vector Control of Interior Permanent Magnet Synchronous Motor over Wide range of Speed using Fuzzy Logic Controller. 2022. Available from: https://ymerdigital.com/uploads/YMER2110C7.pdf.
16) Wu J, Liu J, Guo Z, Wang Y. Fuzzy Single-Current Field Weakening Control of IPMSM in EV. *Authorea Preprints*. 2022. Available from: https://www.authorea.com/doi/full/10.22541/au.165752686.61778568.
17) Wang H, Wang T, Zhang X, Guo L. Voltage feedback based flux-weakening control of IPMSMs with fuzzy-PI controller. *International Journal of Applied Electromagnetics and Mechanics*. 2020;62(1):31–43. Available from: https://doi.org/10.3233/JAE-190014.
18) Tan L, Ping L, Shuai C. A High Performance Speed Control Method Based on Fuzzy-PI of IPMSM for BEV. *Journal of Chongqing Jiaotong University (Natural Science)*. 2019;38(11):139. Available from: https://doi.org/10.3969/j.issn.1674-0696.2019.11.22.